Nanoscale Fibrils and Grids: Aggregated Structures from Rigid-Rod Conjugated Polymers

Jinsang Kim,[†,‡] Sean K. McHugh,[†] and Timothy M. Swager*,[†]

Department of Chemistry and Department of Materials Science and Engineering, Massachusetts Institute of Technology, Cambridge, Massachusetts 02139

Received November 16, 1998

ABSTRACT: Langmuir−Blodgett (LB) molecular processing of conjugated polymers [poly(phenylene ethynylenes)] into highly aligned films has revealed conditions for the formation of liquid crystalline monolayer films that structurally evolve into fibril aggregates. The structural requirements for poly-(phenylene ethynylene)s to display liquid crystalline phases capable or alignment by LB methods were determined. The reconstruction of monolayers into fibril structures was found to require a low glass-transition temperature (T_g), weak surface anchoring, and a monolayer with a high energy that can be stabilized by reorganization. This assembly of polymers into aggregated structures produces rigid structural units analogous to naturally occurring fibrous proteins such as collagen and elastin. These oriented, shape-persistent nanoscale structures create new possibilities for the construction of complex supramolecular structures, and this capability has been demonstrated by the formation of a nanoscale grid.

Introduction

The creation of complex supramolecular structures at interfaces is central to many emerging and established technologies.[1] Given that complex macroscopic structures (buildings, bridges) are generally built from high-aspect rigid structural elements (beams, trusses), it seems only natural to consider molecular analogues (rigid-rod polymers) for the construction of complex supramolecular structures. However, there are many persistent challenges for the organization of these molecular building blocks. Not the least of these problems is that, although a simple chemical drawing would suggest a perfect rod structure, rigid-rod polymers generally exhibit equilibrium flexibility and finite persistence lengths.[2] Nature achieves rigid shape-persistent structures not through a single molecular chain but by the aggregation of molecular building blocks. Examples include the fibrous proteins collagen and elastin,[3] which are structural constituents of biological tissues, and the RNA-templated aggregation of proteins which forms the strucure of the tobacco mosaic virus.

Molecular processing using the Langmuir−Blodgett (LB) deposition technique represents a powerful method for the organization of rodlike polymers.[4] Under ideal circumstances, a Langmuir layer at the air−water interface displays an isothermal phase sequence as a function of surface pressure beginning with a two-dimensional gas, transforming to a two-dimensional liquid, and finally transitioning to a two-dimensional crystal phase. Compressed monolayers can be transferred to a substrate by controlled dipping at a constant surface pressure. Previous LB studies of rigid-rod polymers with a nonpolar "hairy-rod" structure have established that flow induced in the transfer of the monolayer film to the substrate is responsible for the formation of anisotropic polymer films.[5] This ordering indicates that these monolayer films of rigid-rod polymers at the air−water interface display nematic liquid crystalline order. These previous studies have been restricted to hairy-rod polymers,[5] and therefore the structural requirements for the formation of two-dimensional liquid crystalline phases of other polymer architectures have yet to be systematically probed. In the case of a liquid crystalline Langmuir monolayer, the materials should equilibrate rapidly after the application of a mechanical perturbation. Stated differently, the monolayer should behave like an anisotropic liquid when subjected to compression, expansion, or flow. The high aspect ratio of rigid-rod polymers is conducive to the formation of liquid crystalline phases, but this structure can also produce large enthalpic interactions between polymers in the form of π-stacked aggregates. To promote liquid crystalline behavior in any system, a delicate balance of repulsive and attractive forces must be maintained.
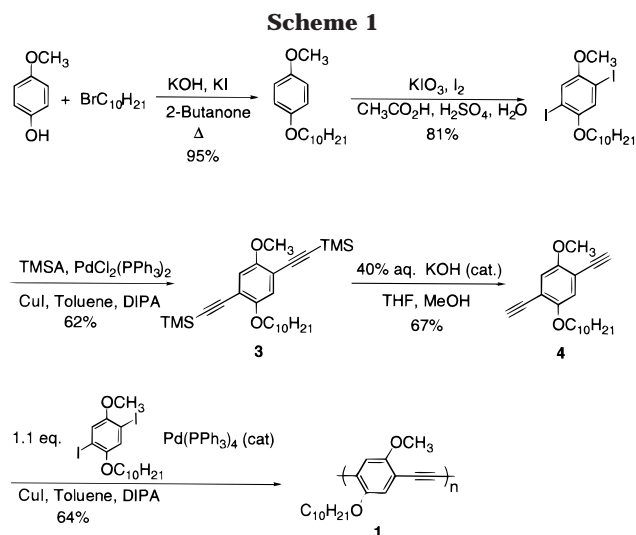
We are exploring the structure−property correlations of monolayers and multilayers formed from conjugated poly(phenylene ethynylene)s. These materials have been shown to behave as exceptional antennas for the transport of optical excitations over long distances[6,7] and can also display high electrical conductivities under carefully controlled conditions.[8] In this contribution, we detail investigations of two surfactant-like poly(phenylene ethynylene)s, **1** (M_n = 13 940, PDI = 3.2) and **2**
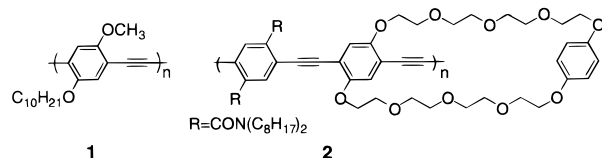
(M_n = 81 200, PDI = 3.4).[9] Our studies are directed at establishing critical design principles for the formation of liquid crystalline films at the air−water interface. An unexpected outcome of our studies has been the observation that under select conditions monolayers reconstruct after deposition into highly anisotropic aggregated nanoscopic fibril networks. These electronic polymer networks form structures only tens of nanom-

† Department of Chemistry.
‡ Department of Materials Science and Engineering.

Scheme 1

Figure 1. Pressure−area isotherms of **1** and **2** at the air−water interface. The area per molecule is determined from the extrapolated area. (b) Compression−expansion cycles showing that multilayer films of **1** do not readily reassemble into monolayers, whereas **2**'s films rapidly equilibrate into monolayer structures upon expansion.

eters in diameter but give interconnected structures which have macroscale (centimeter) dimensions along the fibril's axis. The special conditions required to achieve this assembly process have been elucidated, and the power of this method is demonstrated in the construction of nanoscale grids.

Results and Discussion

The synthesis of polymer **1** begins with commercially available *p*-methoxyphenol in a Williamson ether synthesis with 1-bromodecane to give *p*-decyloxyanisole in 95% yield (Scheme 1). Standard iodination procedures were used to iodinate the aromatic ring in the ortho positions to give 2,5-diiodo-4-decyloxyanisole in 81% yield. The coupling of 2 equiv of (trimethylsilyl)acetylene to the diiodide using palladium catalysis produced **3** (62%), which was then converted to the terminal acetylene **4** (67%) using a catalytic amount of 40% aqueous KOH solution in a tetrahydrofuran and methanol mixture. The coupling of terminal acetylene **4** with 2,5-diiodo-4-decyloxyanisole using tetrakis(triphenylphosphine)palladium afforded the rigid-rod polymer **1**. It was necessary to use an offset stoichiometry (0.9 diiodide to 1.0 diacetylene) to obtain polymers of lower molecular weight. Initial reactions using the standard 1 equiv of diiodide to 1.0−1.03 equiv of diacetylene gave insoluble polymers.

Neither **1** nor **2** are classical surfactants, which typically have charged headgroups, but they have structural components that can be ranked as more or less polar. The methoxy groups of **1** are the polar portion of the macromolecule, and the decyloxy groups constitute the nonpolar tails. For **2**, the dioctyl amide groups are decidedly less polar than the polyether macrocycle. These different structural attributes lead to very different organizations at the air−water interface, a feature readily apparent from the pressure−area isotherms shown in Figure 1. These studies reveal an extrapolated area of 32 Å^2 per repeating unit for **1**, a value much smaller than that observed for **2**, which displays an area of about 210 Å^2 per repeat.[11] This large difference is accounted for by considering that **1** organizes with the plane of its π system perpendicular to the air−water interface, whereas **2** prefers to organize with the plane of its aromatic rings parallel to the interface (Chart 1). This orientation is consistent with X-ray[12] and ellipsometric analyses of multilayer films,
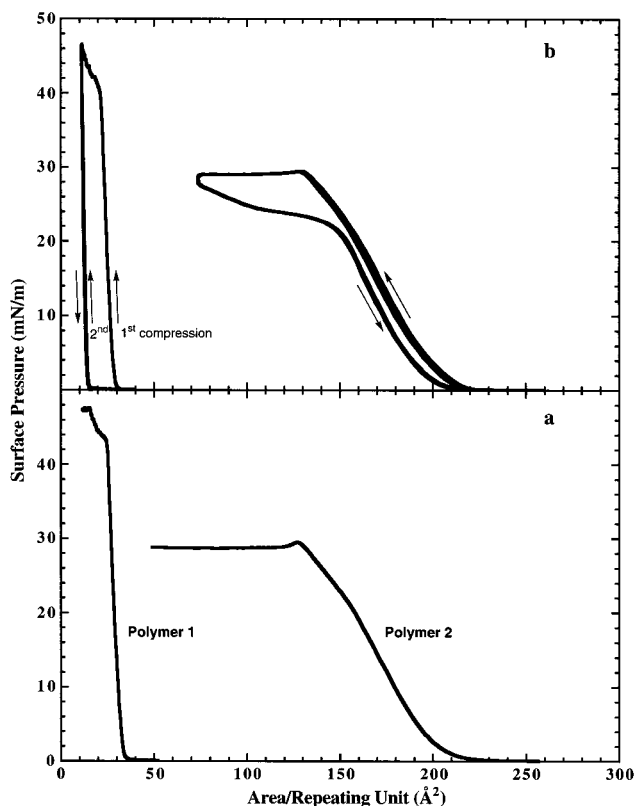
which show a linear incremental increase in the film thickness of 11 Å per monolayer for **2** and a somewhat higher thickness of 18 Å per monolayer for **1**. These differences also lead to contrasting film-forming characteristics for **1** and **2**. Visual inspection of Langmuir monolayers with a polarized optical microscope reveals that **1** displays an aggregated structure prior to compression. Alternatively, **2** appears to uniformly distribute over the entire surface in a gaslike state prior to compression.

Other characteristics of the films also support the orientation in Chart 1. For example, **1** lacks compressibility as indicated by a steep slope of the pressure−area isotherm, whereas films of **2** are very compressible. Additionally, **1** tolerates a higher pressure (43 mN/m) before folding into multilayers than **2**, which transforms to a multilayer structure at pressures over 29mN/m. These contrasting properties are the result of different intermolecular interactions. Polymer **2**'s edge-on interpolymer contacts, which are between conformationally flexible alkyl and polyether chains, are weak and easily deformed, whereas **1** is arranged in a rigid crystalline π-stacked structure. The electronic spectrum also indicates differences in interchain interactions, and **1**'s absorption λ_{max} in solution phase at 449 nm shifts to 487 nm in monolayer structures.[13] On the other hand, **2**'s absorption λ_{max} is only slightly shifted from a value of 424 nm in solution to 434 nm in monolayers.

The degree of association between polymer chains and free volume are critical determinants of a polymer's dynamics. The differences between **1** and **2**'s dynamics are readily evident when monolayers are compressed
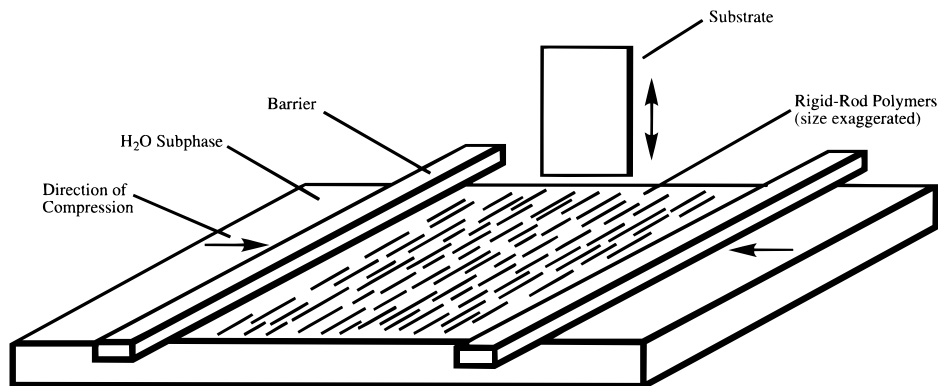
Figure 2. LB deposition geometry providing the best alignment. Anisotropic compression of the two-dimensional liquid crystalline film produces order that is further enhanced by flow resulting from the dipping process.

Chart 1
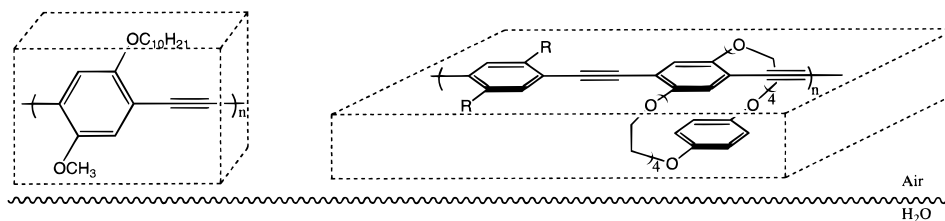
into multilayers, reexpanded, and then subjected to recompression (Figure 1b). For **1**, multilayer formation is not reversible, and the repeated compression showed a much smaller area per repeating unit. For **2**, however, expansion of multilayers regenerates a monolayer film, and the second compression produces the same pressure−area isotherm. The pressure initially drops with expansion, but this hysteresis in **2**'s pressure−area profile is independent of the compression−expansion rate from 2 to 50 cm^2/min and is therefore an artifact of the pressure measurement rather than true kinetic behavior. The differences in dynamics between the two materials are also reflected in their glass transition temperatures (T_g), which were 184 and −3 °C for **1** and **2**, respectively.[14] Neither polymer displayed a melting transition (DSC) up to a temperature of 250° C, suggesting the absence of any crystalline phase. Our investigations all support the assignment of **1** displaying a two-dimensional crystal phase and that compressed monolayers of **2** display a two-dimensional liquid crystal phase.

Alignment of the polymer monolayers can occur as a result of both anisotropic compression and the flow generated during the transfer to a substrate. There is a natural tendency of rigid rods to align perpendicular to the direction of compression and parallel to lines of flow between the water and the substrate induced by dipping.[15,16] An optimized deposition geometry (in a standard LB trough) places the plane of the substrate parallel to the direction of compression (Figure 2). The anisotropy is readily quantified by measuring the polarized optical absorption of deposited films, because for both polymers the absorption at λ_{max} is polarized along the polymer axis. The polymers always align parallel to the dipping direction and 10 multilayer films of **1** exhibited a modest anisotropy ($A\|/A\perp = 3.4$), whereas **2** displayed higher values ($A\|/A\perp = 6.3$) comparable to films produced previously by the LB technique in carefully optimized flow fields.[5] Alternate orientation of the substrate plane normal to the direction of compression produced films with lower optical anisotro-

pies for **2** ($A\|/A\perp = 1.8$ to 2.1). In this case, the polymers still aligned in the dipping direction, thereby indicating that flow-induced alignment dominates.

The transfer of monolayers to a substrate in the LB method is determined by the hydrophilic or hydrophobic nature of the substrate. A hydrophobic surface is required to best deposit a monolayer on a single downward stroke. Alternatively, a monolayer can be efficiently deposited with an upward stroke on a hydrophilic surface. In the former, monolayers have only weak anchoring to the surface, but H-bonding interactions in the latter produces strong anchoring. The monolayers were deposited in a compressed state at pressures below those at which the collapse to form multilayers occurs, (20 and 18 mN/m for **1** and **2**, respectively). Polymer **1** displays quantitative transfer characteristics (>95%) over many dipping cycles. In contrast, **2** displays alternating transfer characteristics wherein a complete transfer is observed on the first downward dip of a hydrophobic substrate,[17] but after the initial upward stroke, which is also quantitative to form a bilayer structure, all other downward dips resulted in less than a 10% transfer ratio. Nevertheless, all subsequent upward strokes result in quantitative (>95%) transfer. The fact that polymer **2** does not transfer significantly (<10%) on downstrokes following an upstroke suggests that only a highly hydrophobic substrate will effect quantitative transfer.

Atomic Force Microscopy (AFM) reveals a smooth, nearly featureless, structure for the bare substrates and for all of the monolayer films except those wherein **2** is deposited on hydrophobic substrates (Figure 3). The latter were prepared with a single downward dip, thereby orienting the polar macrocyclic moieties outward. Close analysis of the AFM images in Figure 3 suggest that **2**'s "mountainous" features are not single polymers but aggregated fibrils 17−30 nm in diameter. The most frequent interfibril distance was determined by two-dimensional Fourier transform analysis to be 20 nm. AFM analysis of monolayers, wherein part of the film was physically removed from the surface to provide
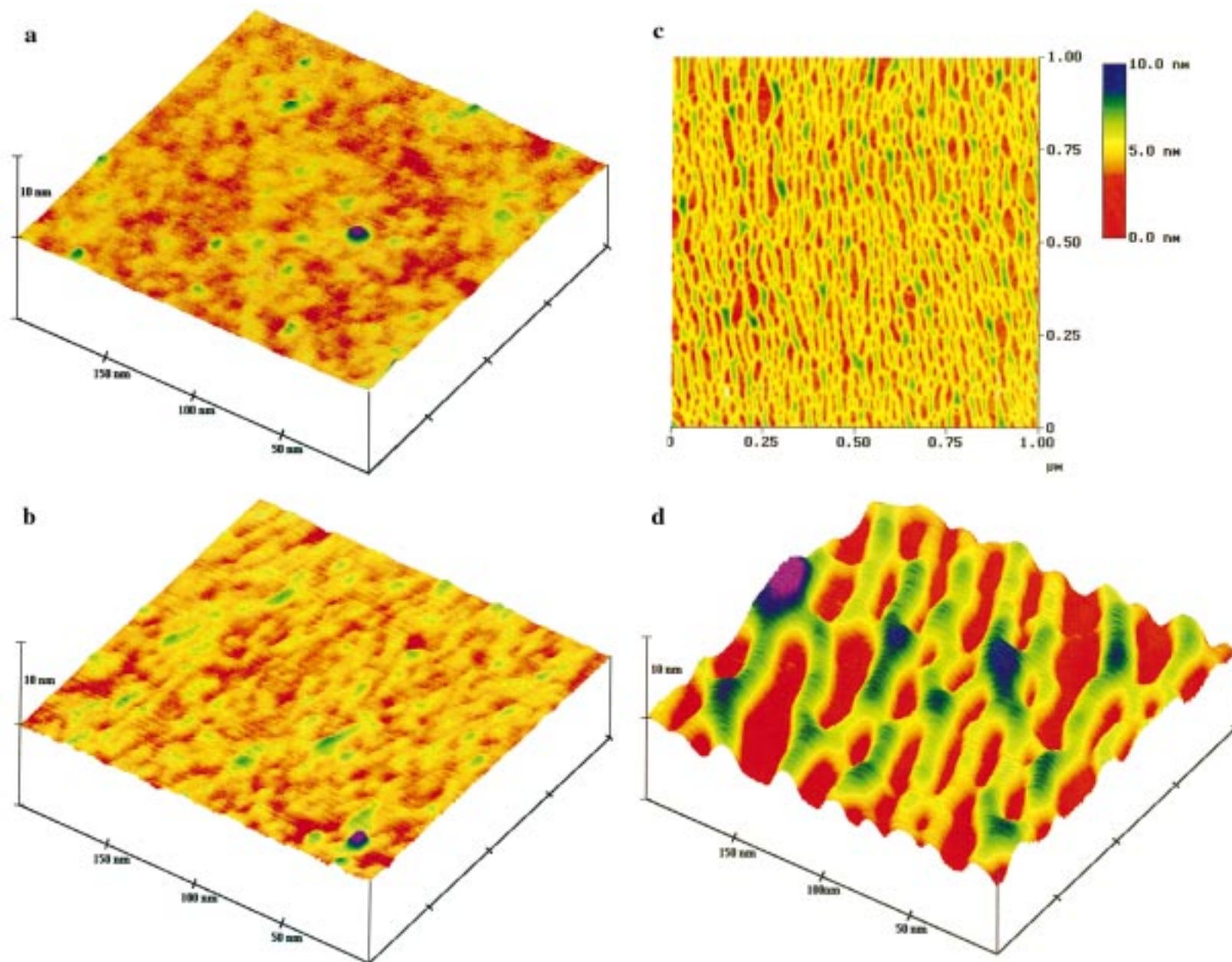
Figure 3. Atomic force images acquired in tapping mode (x, y, and z scales given) of a (a) bare HMDS-treated Si substrate; (b) monolayer of **2** deposited with an upstroke onto a hydrophilic substrate; (c) topological large area view; and (d) three-dimensional view of the reconstructed fibril structure from a monolayer of **2** deposited with a downstroke on a hydrophobic substrate.

a reference region of bare substrate, established that the "valley floors" are the bare Si substrate. The height of the mountainous features ranges from 1.6 to 2.6 nm, and the most frequent value was 2.0 nm. This value is about twice the thickness obtained by the XRD and ellipsometry and is consistent with our model for reconstruction of the monolayer (vide infra). In the case of multilayer deposition, the first layer is not allowed to reconstruct because a second layer is deposited on the immediate upstroke. The fact that we do not see a reconstructed structure in monolayer films of **2** prepared on a hydrophilic substrate by a single upward stroke is a consequence of strong anchoring via hydrogen bonds to the surface. Additionally, **1** does not display a similar reconstruction because its crystalline structure lacks mobility. We have confirmed the degree of surface anchoring with thermal annealing studies at 90 °C as a function of time. These studies show monolayers of **2** on hydrophobic substrates to decline more rapidly in electronic anisotropy than do monolayers on hydrophilic substrates. Extended heating (7 days) showed the former to transform to a droplet structure, whereas the latter remained planar.

Polar surfaces are high-energy species, and molecular dipoles at the air−substrate interface can obtain lower energy structures by reorganizing in a way that produces a more nonpolar surface. The high energy of the initial monolayer of **2** formed after transfer to a hydrophobic surface is the driving force responsible for its reconstruction into a fibrillar structure. The degree of hydrophobicity of the surfaces is a measure of polarity and can be interrogated by contact-angle measurements. The virgin hydrophobic 1,1,1,3,3,3-hexamethyldisilazane (HMDS) coated Si surfaces exhibit a contact angle of 108°. Consistent with **1**'s nonpolar structure, its monolayers display a hydrophobic character, 93° and 96°, when deposited on hydrophobic or hydrophilic substrates, respectively. Monolayers of **2** deposited on hydrophilic substrates display a 63° contact angle. Films of **2** deposited on hydrophobic substrates display a higher contact angle of 75°. It was initially surprising to find that the latter films, which should present the more polar cyclophane groups, were less polar than those which should present the dioctyl amides. This fact and consideration of the surface energy points to a surface reconstruction in which the polar macrocycles are placed in the interior of the fibril with the nonpolar side chains coating the exterior fibril surface (Scheme 2).

The ability to create nanoscopic aligned fibrils from conjugated polymers provides new opportunities to realize the potential of rigid-rod polymers for the construction of complex functional supramolecular architectures. As a first demonstration of this principle, we have prepared bilayer structures wherein two layers of fibrils are aligned in a perpendicular arrangement to form a grid. These structures are formed by first dipping a hydrophobic substrate and removing the remaining Langmuir film while keeping the substrate submerged. The substrate with a transferred polymer monolayer is then removed from the LB apparatus, rotated 90°, and then dipped downward through a fresh Langmuir film. This rotation takes about 10 min, which appears to be adequate time for the reconstruction of the first monolayer. A quantitative transfer (>95%) for the second downstroke indicates that the fibrillar structure from the first monolayer has sufficient hy-

Scheme 2

Edge Views of Polymer **2**
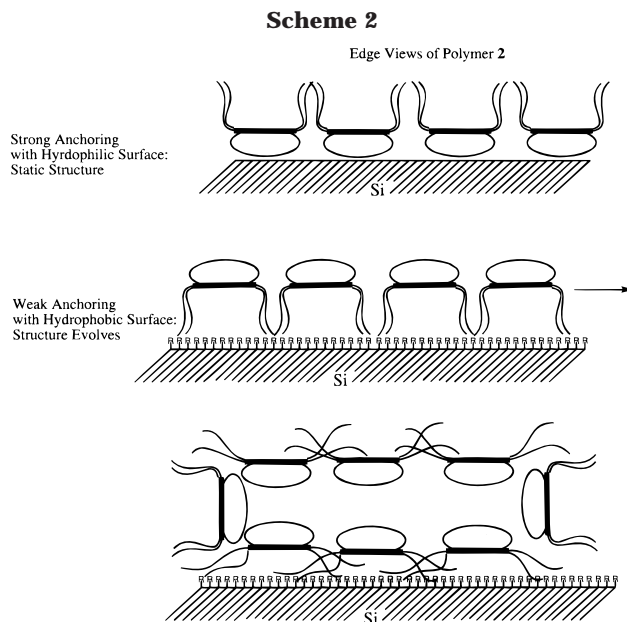
drophobic character. Recall from contact-angle measurements that the reconstructed fibril surface displayed a greater hydrophobicity than films prepared on a upstroke, which were ineffective at transferring a monolayer. The Langmuir film is again removed with the substrate submerged. AFM of the resultant bilayer film shows (Figure 4) the second monolayer to undergo a similar reconstruction into a fibril structure and thereby produce a grid structure.

As can be seen in Figure 4a, the second layer, oriented horizontally, has its highest elevation at the intersection between the fibrils. Given the low T_g of **2**, one might expect the polymer chains to interdiffuse at these intersections. However, the chain alignment and the rigid-rod character of the polymers inhibits the interdiffusion of the polymer's perpendicularly oriented fibrils. The three-dimensional view of the grid also shows that the fibrils have effectively collapsed into the valleys created by the first fibril layer. The individual molecules are flexible, and the polymers are not crosslinked in the fibrils. Hence, the structures have deformed to create a conformal arrangement. The nanoscale pores extend to the bare surface and are on average rectangular in shape. This shape is a result of the fact that the second monolayer tends to assemble into larger fibrils and thereby produces a bigger spacing between fibers. Attempts to use two-dimensional Fourier transforms to extract the characteristic length scales were unsuccessful. However, section analysis of AFM images showed the first layer to have the same characteristic length scale (ca. 20 nm) as was determined on the simple monolayer structure. Section analysis of the second layer showed the fibrils to be wider (ca. 38 nm) and to have an average interfibril spacing of 42 nm. This larger periodicity, which requires a larger average displacement of the polymer chains, is likely the result of a higher mobility of the second layer provided by a reduction in the number of surface contacts that the polymer fibrils exhibits.

Outlook. Assemblies of electronically active polymers such as shown here offer a number of opportunities in supramolecular science.[18] Tailor-made supermolecular nanoscopic structures are of interest for size selection of large biological molecules, chemical sensors, and
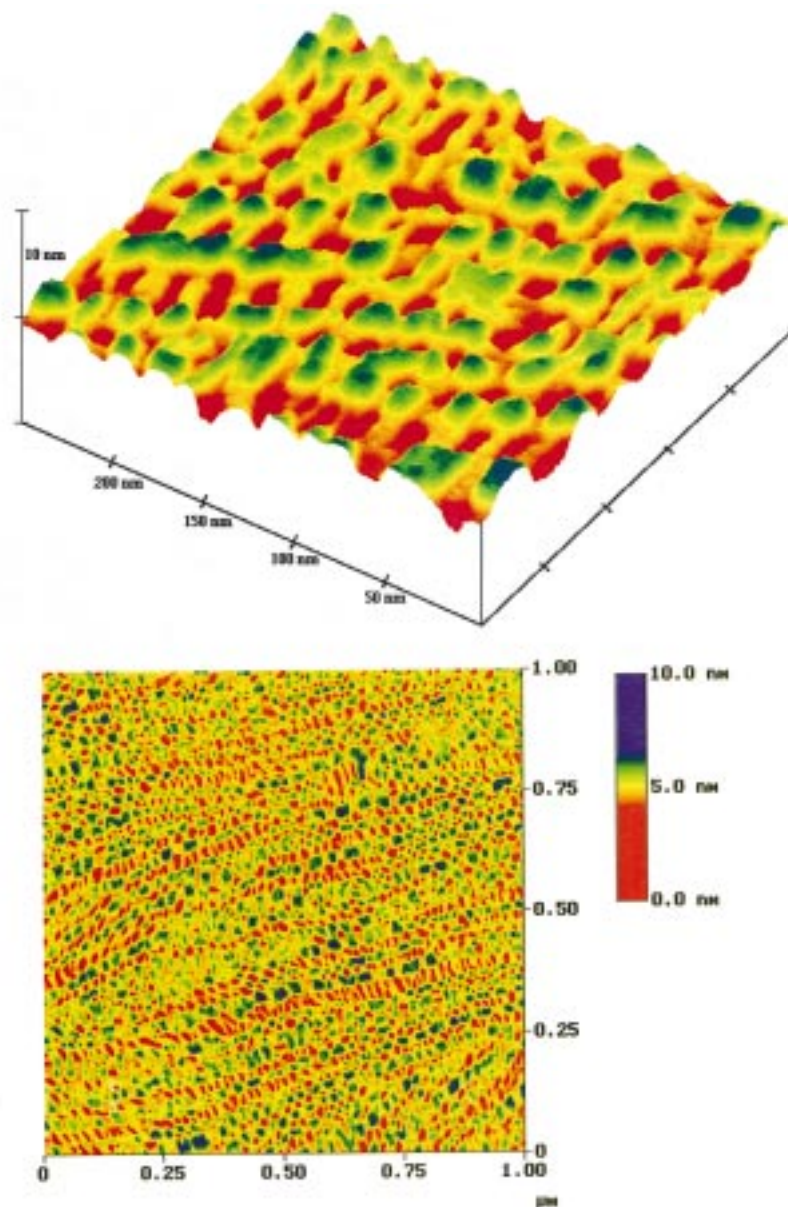
Figure 4. Atomic force images acquired in tapping mode (*x*, *y*, and *z* scales given) of three-dimensional grid patterns described in the text. (a) Three-dimensional view (200 × 200 × 20 nm). (b) Topological view (1 × 1 μm).

molecular electronics. The addition of biological receptors or ligands to similar conjugated polymers can induce the docking of biomolecules in the subphase for the creation of new postdeposition structures or environments. Hybrid monolayer and multilayer assemblies are likely to reveal a host of new structures.

Experimental Section

General Methods. Air- and moisture-sensitive reactions were carried out in flame-dried glassware using standard Schlenk line or drybox techniques under an inert atmosphere of dry argon. All chemicals used were of reagent grade and were purchased from Aldrich unless otherwise noted. Anhydrous toluene was used from Aldrich Kilo-lab metal cylinders. CH_2Cl_2 and THF were used directly from Aldrich Sure-seal bottles. Diisopropylamine was distilled over solid KOH pellets and degassed by three freeze−pump−thaw cycles. Tetrakis-(triphenylphosphine)palladium (0) and *trans*-dichlorobis(triphenylphosphine)palladium(II) were purchased from Strem chemicals and used as received. Polymer **2** was prepared by the literature procedure.[10] (Trimethylsilyl)acetylene was purchased from Farchan Laboratories and used as received. [1]H

NMR spectra were acquired at 250 or 300 MHz, and ^{13}C NMR spectra were obtained on a 500 MHz (125.66 MHz ^{13}C) spectrometer. ^{1}H and ^{13}C NMR spectra were taken in $CDCl_3$ with ^{1}H chemical shifts reported relative to internal tetramethylsilane (0.00 ppm) and ^{13}C chemical shifts reported relative to $CDCl_3$ (77.00 ppm).

Polymer molecular weights were determined with a Hewlett−Packard 1100 series HPLC equipped with a PL gel mixed-C column (5 μ) using THF as the mobile phase at a rate of 1 mL/min. Gel permeation chromatography (GPC) measurements were made relative to monodisperse polystyrene standards purchased from Polymer Laboratories. It is important to note that for rigid-rod polymers this technique often provides relative molecular weights higher than the actual values. UV−vis spectra were obtained on a Hewlett−Packard 8453 diode array spectrophotometer. IR measurements were performed with a Nicolet Impact 410 FT-IR spectrometer. A Nima 601M model LB trough (Aspect ratio, 2:1 length/width) equipped with a vertical dipping mechanism was used for all deposition and analytical studies. Water in the subphase was purified with a Barnstead Nanopure system and had a conductivity of 18.3 MΩ. Substrates were 18 × 18 mm glass microscope cover slides or 15 × 18 mm pieces of a silicon wafer. All substrates were

sonicated in a detergent solution for 20 min, rinsed twice with subphase quality water, and then sonicated twice with subphase quality water for 20 min. After sonication, the substrates were dried with hot air and further dried for 2 h under high vacuum. To give the substrate a hydrophobic surface property, the purified substrates were left in a sealed chamber with HMDS (Aldrich, 99.9%) for 12 h and then stored under vacuum. For hydrophilic surfaces, the pretreated substrates were sonicated in concentrated nitric acid for 20 min, and then washed twice with subphase quality water before being sonicated in a 5 mM solution of sodium hydroxide for 20 min. These hydrophilic substrates were then subjected to a double rinse with subphase quality water and dried under high vacuum. Polymer solutions in chloroform (1 mg/mL) were spread on a water–air interface. After 2–3 min were allowed for the evaporation of the solvent, the monolayer was compressed by two barriers with a constant speed of 25 cm^2/min until a target pressure was attained. The monolayers were annealed by three subsequent cycles of expansion and compression. Monolayers were then transferred to the substrate at a dipping speed of 10 mm/min while the target pressure was held constant. The resulting LB films were dried under vacuum for about 1 h prior to characterization.

The AFM images were recorded using tapping mode on a Nanoscope III from Digital Instruments, Inc. The thickness measurement for multilayer LB films was done by using a laser operating at 633 nm with a ellipsometer from Gaertner Scientific Corporation. The thickness of three film locations were determined and averaged. Advancing contact angles were measured by adding water very slowly to a water drop on the LB films using a Video Contact Angle System 2000 from Advanced Surface Technology, Inc. Contact angles of three film locations were averaged. The XRD thickness measurements were performed using Rigaku RU 300. The data were obtained by using a wavelength of 1.54 Å from a Cu anode. The Kiessig fringes from multilayers were obtained, and the thickness per layer was calculated from the number of layers

***p*-Decyloxyanisole.** A 1-L, three-necked round-bottomed flask equipped with a stir bar and a condenser was charged with *p*-methoxyphenol (32.98 g, 0.27 mol, 0.98 equiv), 1-bromodecane (56.25 mL, 0.27 mol, 1 equiv), potassium hydroxide (30.79 g, 0.55 mol, 2 equiv), potassium iodide (5.86 g, 40 mmol, 0.13 equiv), and 2-butanone (500 mL). The reaction mixture was heated to reflux for 24 h. After being cooled to room temperature, the mixture was partitioned between diethyl ether (750 mL) and water (500 mL). The organic layer was separated, washed sequentially with saturated aqueous NH$_4$-Cl (2 × 500 mL) and water (500 mL), dried (MgSO$_4$), and concentrated in vacuo. Recrystallization from THF–MeOH afforded *p*-decyloxyanisole as large white plates (68.10 g, 95%, mp 49–50 °C): ^{1}H NMR (300 MHz, CDCl$_3$) δ 6.83 (s, 4H), 3.89 (t, *J* = 6.6 Hz, 2H), 3.76 (s, 3H), 1.75 (qn, *J* = 6.6 Hz, 2H), 1.5–1.2 (br m, 14H), 0.88 (t, *J* = 6.9 Hz, 3H); ^{13}C NMR (125 MHz, CDCl$_3$) δ 153.83, 153.50, 115.57, 114.76, 68.81, 55.85, 32.11, 29.81, 29.78, 29.64, 29.61, 29.54, 26.28, 22.89, 14.31; IR (KBr, cm^{-1}) 2955, 2919, 2850, 1513, 1243. Anal. Calcd (C$_{17}$H$_{28}$O$_2$): C, 77.22; H, 10.67. Found: C, 77.47; H, 10.49.

2,5-Diiodo-4-decyloxyanisole. A 3 L, three-necked round-bottomed flask equipped with a stir bar and a condenser was charged with *p*-decyloxyanisole (30.79 g, 0.12 mol, 1 equiv), potassium iodate (10.00 g, 50 mmol, 0.41 equiv), and iodine (32.60 g, 0.13 mol, 1.11 equiv). Glacial acetic acid (1200 mL), concentrated sulfuric acid (12 mL), and water (120 mL) were added, and the mixture heated to reflux for 2 days. After being cooled to room temperature, the excess iodine was quenched with 10% aqueous Na$_2$S$_2$O$_4$ (500 mL). The resulting mixture was further diluted with water (500 mL) and filtered, and the solid was dissolved in CH$_2$Cl$_2$ (750 mL). The organic layer was washed sequentially with 10% aqueous Na$_2$S$_2$O$_4$ (100 mL) and saturated aqueous NaCl (100 mL), dried (MgSO$_4$), and concentrated in vacuo. Recrystallization in CH$_2$Cl$_2$–MeOH afforded the title compound as white needles (48.60 g, 81%, mp 56.5–57.5 °C): ^{1}H NMR (250 MHz, CDCl$_3$) δ 7.19 (s, 1H), 7.18 (s, 1H), 3.93 (t, *J* = 6.4 Hz, 2H), 3.82 (s, 3H), 1.80 (qn, *J* = 8.1 Hz, 2H), 1.55–1.20 (br m, 14H), 0.88 (t, *J* = 6.3 Hz, 3H); ^{13}C

NMR (125 MHz, CDCl$_3$) δ 153.17, 152.92, 122.88, 121.44, 86.34, 85.41, 70.34, 57.13, 31.86, 29.51, 29.50, 29.28, 29.24, 29.11, 25.99, 22.65, 14.09; IR (KBr, cm^{-1}) 2962, 2919, 2849, 1485, 1215. Anal. Calcd (C$_{17}$H$_{26}$O$_2$I$_2$): C, 39.56; H, 5.08. Found: C, 39.49; H, 5.22.

2,5-Bis[(trimethylsilyl)ethynyl]-4-decyloxyanisole (3). A 250 mL Schlenk flask equipped with a stir bar was charged with 2,5-diiodo-4-decyloxyanisole (20.00 g, 40 mmol, 1 equiv), *trans*-dichlorobis(triphenylphosphine)palladium(II) (0.82 g, 1.20 mmol, 0.03 equiv), and copper(I) iodide (0.46 g, 2.4 mmol, 0.06 equiv). The flask was placed under argon, and then toluene (250 mL) and diisopropylamine (14.0 mL, 0.10 mol, 2.5 equiv) were successively added by syringe. The deep red solution was treated with (trimethylsilyl)acetylene (13.0 mL, 90 mmol, 2.2 equiv) and stirred for 48 h at room temperature. The black mixture was concentrated in vacuo, and the residue dissolved in hexanes. The hexanes solution was filtered through a 1 in. plug of silica gel and eluted with chloroform. The solvent from the filtrate was once again evaporated, and the resulting solid was recrystallized (methanol) to afford **3** as yellow needles (11.05 g, 62%, mp 72–73 °C): ^{1}H NMR (250 MHz, CDCl$_3$) δ 6.91 (s, 1H), 6.89 (s, 1H), 3.95 (t, *J* = 6.3 Hz, 2H), 3.83 (s, 3H), 1.79 (qn, *J* = 8.2 Hz, 2H), 1.50–1.15 (br m, 14H), 0.88 (t, *J* = 6.9 Hz, 3H), 0.27 (s, 18H); ^{13}C NMR (125 MHz, CDCl$_3$) δ 154.14, 154.07, 117.83, 113.39, 101.01, 100.90, 100.18, 100.15, 69.49, 56.36, 31.86, 29.61, 29.56, 29.40, 29.35, 29.30, 26.00, 22.65, 14.07, −0.02, −0.07; IR (KBr, cm^{-1}) 2956, 2923, 2858, 2152, 1497, 1225, 841. Anal. Calcd (C$_{27}$H$_{44}$O$_2$Si$_2$): C, 70.99; H, 9.71. Found: C, 70.65; H, 9.73.

2,5-Diethynyl-4-decyloxyanisole (4). A 250 mL round-bottomed flask equipped with a stir bar was charged with 2,5-bis[(trimethylsilyl)ethynyl]-1-methoxy-4-decyloxybenzene (**3**) (5.14 g, 10 mmol), THF (40 mL), and methanol (20 mL). The flask was capped, and argon was bubbled through the solution for 30 min. The reaction mixture was treated with an oxygen-free 40% aqueous KOH solution (2 mL), stirred for 19 h, and then poured into hexanes (200 mL). The organic solution was washed with water (3 × 100 mL), dried (MgSO$_4$), and concentrated in vacuo. The resulting residue dissolved in hexanes–CH$_2$Cl$_2$ (1:1) and was filtered through a 1 in. plug of silica gel. The filtrate was once again concentrated in vacuo, and the resulting solid was recrystallized from hexanes to afford **4** as light yellow needles (2.36 g, 67%, mp 64.5–65.5 °C): ^{1}H NMR (250 MHz, CDCl$_3$) δ 6.97 (s, 1H), 6.96 (s, 1H), 3.98 (t, *J* = 6.7 Hz, 2H), 3.86 (s, 3H), 3.39 (s, 1H), 3.35 (s, 1H), 1.81 (qn, *J* = 7.9 Hz, 2H), 1.53–1.12 (br m, 14H), 0.88 (t, *J* = 6.9 Hz, 3H); ^{13}C NMR (125 MHz, CDCl$_3$) δ 154.31, 154.07, 117.95, 115.98, 113.37, 112.55, 82.55, 82.52, 79.70, 69.70, 56.35, 31.88, 29.54, 29.51, 29.30, 29.11, 25.87, 22.65, 14.08; IR (KBr, cm^{-1}) 3279, 2925, 2849, 1488, 1216. Anal. Calcd (C$_{21}$H$_{28}$O$_2$): C, 80.73; H, 9.03. Found: C, 81.02; H, 9.29.

Polymer (1). A 25 mL Schlenk flask equipped with a stir bar was charged with 2,5-diiodo-4-decyloxyanisole (200 mg, 0.39 mmol, 1 equiv), 2,5-diethynyl-4-decyloxyanisole (**4**) (0.107 g, 0.34 mmol, 0.9 equiv), and copper(I) iodide (5.5 mg, 29 μmol, 0.06 equiv). The flask was placed under argon, and tetrakis(triphenylphosphine)palladium(0) (15 mg, 13 μmol, 0.03 equiv) was added under a nitrogen atmosphere. Diisopropylamine (1.25 mL, 8.9 mmol, 23 equiv) and toluene (3.5 mL) were successively added by syringe, and the mixture was stirred at room temperature for 30 min. The fluorescent yellow mixture was heated to 60 °C, stirred for 14 h, and then cooled to room temperature. The resulting polymer was precipitated in acetone (100 mL), filtered, and rinsed with hot ethanol and hexanes to afford **1** as an amorphous yellow solid (141 mg, 63%): ^{1}H NMR (300 MHz, CDCl$_3$) δ 7.05 (m, 2H), 4.05 (br m, 2H), 3.92 (m, 3H), 1.86 (m, 2H), 1.52 (m, 2H), 1.41–1.08 (br, 12H), 0.87 (t, *J* = 6.6 Hz, 3H); ^{13}C NMR (125 MHz, CDCl$_3$) δ (including low intensity peaks corresponding to end groups) 153.92, 153.85, 153.72, 153.55, 117.52, 117.33, 115.5–115.1, 91.8–91.2, 69.78, 69.74, 69.68, 69.64, 56.52, 56.46, 56.39, 31.90, 29.69–29.57, 29.51–29.41, 29.40–29.28, 26.03, 26.01, 25.98, 25.95, 29.67, 14.09; GPC M_w = 44 818, M_n = 13 940; PDI = 3.2.

References and Notes

(1) Ulman, A. *An Introduction to Ultrathin Organic Films: From Langmuir−Blodgett to Self-Assembly*; Academic Press: Boston, 1991.

(2) Light scattering studies on polymers closely related to those in this study have revealed a presistance length, based upon a wormlike chain model, of 15 nm. Cotts, P. M.; Swager, T. M.; Zhou, Q. *Macromolecules* **1996**, *29*, 7323.

(3) *Fibrous Protein Structure*; Squire, J. M., Vibert, P. J., Eds.; Academic Press: San Diego, 1987.

(4) Wegner, G. *Thin Solid Films* **1992**, *216*, 105.

(5) Schweigk, S.; Vahlenkamp, T.; Xu, Y.; Wegner, G. *Macromolecules* **1992**, *25*, 2513.

(6) Zhou, Q.; Swager, T. M. *J. Am. Chem. Soc.* **1995**, *117*, 7017.

(7) For detailed photophysical and energy-transport studies of the films reported herein, see: Levitsky, I. A.; Kim, J.; Swager, T. M. *J. Am. Chem. Soc.*, in press.

(8) Ofer, D.; Swager, T. M.; Wrighton, M. S. *Chem. Mater.* **1995**, *7*, 418.

(9) Polymer **2** was synthesized as reported previously in ref 10.

(10) Zhou, Q.; Swager, T. M. *J. Am. Chem. Soc.* **1995**, *117*, 12593.

(11) The areas are given in terms of a repeating unit, which involves one phenylene ethynylene group for **1** and two phenylene ethynylene groups for **2**.

(12) X-ray determination of the thickness was performed by analysis of Kiessig fringes.

(13) The π-stacked structure is also consistent with the fact that **1**'s fluorescence is noticeably lower in films than in solution, which is expected for a highly symmetric aggregated conjugated polymer. See: Cornil, J.; dos Santos, D. A.; Crispin, X.; Silbey, R.; Brédas, J. L. *J. Am. Chem. Soc.* **1998**, *120*, 1289.

(14) Glass-transition temperatures (T_g) were determined on bulk samples by differential scanning calorimetry (DSC) (10 °C/min).

(15) Studies have established the relationship of the lines of flow with the alignment of monolayers. See: ref 5. Mareyama, T.; Friedenberg, M.; Fuller, G. G.; Frank, C. W.; Robertson, C. R.; Wegner, G. *Thin Solid Films* **1996**, *273*, 76.

(16) *Liquid Crystallinity in Polymers: Principles and Fundamental Properties*; Ciferri, A., Ed.; VCH: Publishers: New York, 1991.

(17) Hydrophobic substrates were produced by treating cleaned Si or glass surfaces with with HMDS.

(18) Bjørnholm, T.; Greve, D. R.; Reitzel, N.; Hassenkam, T.; Kjaer, K.; Howes, P. B.; Larsen, N. B.; Bøgelund, J.; Jayaraman, M.; Ewbank, P. C.; McCullough, R. D. *J. Am. Chem. Soc.* **1998**, *120*, 7643.

MA981774R